DYNAMIC LIGHT SCATTERING FROM POLYDISPERSE SUSPENSIONS OF LARGE SPHERES

Characterization of Isolated Secretory Granules

SATORU FUJIME, MICHIHO TAKASAKI-OHSITA, AND SHIGEAKI MIYAMOTO
Mitsubishi Kasei Institute of Life Sciences, Machida, Tokyo 194, Japan

ABSTRACT Dynamic light scattering is useful in determining the diameter of submicrometer particles in suspension. When both static scattering intensity $P(K)$ and apparent diffusion coefficient D can be measured in a wide range of the length of the scattering vector $\mathbf{K}$, it is possible to determine the number-average diameter d_n and sharpness in size distribution of spheres. We derived approximate, but very simple, expressions for $\langle P(K)\rangle$ and $\langle D\rangle/D(d_n)$ applicable to very large spheres for which the so-called Rayleigh-Debye condition is perturbed, where $\langle\ldots\rangle$ stands for the size average. These approximate expressions were compared with the numerical results based on the Mie scattering theory. Experimental results for isolated secretory granules, zymogen ($d_n \sim 800$ nm) and chromaffin ($d_n \sim 400$ nm) granules, were analyzed by use of the present formulation, and the dispersion in size distribution, $\sigma/d_n = [(\text{the mean of } d^2)/d_n^2 - 1]^{1/2}$, was found to be about 0.2 for both types of granules.

INTRODUCTION

The elastic modulus of membrane can be determined by an osmotic swelling method, when the membrane forms a vesicle (Li et al., 1986; Miyamoto et al., 1988). The key step in this method is the determination of the vesicle diameters d_0 at $\Delta P = 0$ and d_f at $\Delta P \neq 0$, where ΔP is the osmotic pressure difference across the wall of the vesicle. For vesicles with submicrometer sizes, a dynamic light-scattering method is the most suitable for determining their diameter. General background information about dynamic light scattering is found in standard textbooks (Chu, 1974; Berne and Pecora, 1975). For a monodisperse suspension of spheres, the field correlation function of the scattered light has a form of $g^1(\tau) = \exp(-DK^2\tau)$, where D is the translational diffusion coefficient of a sphere, $K = (4\pi n_2/\lambda_0)\sin(\theta/2)$ is the length of the scattering vector (n_2, the refractive index of the medium; λ_0, the wavelength of the incident light in vacuum; and θ, the scattering angle), and τ is the delay time. From the decay rate of the correlation function, we obtain D, and hence the particle diameter d from $D = k_BT/(3\pi\eta d)$, where k_B is the Boltzmann constant, T is the absolute temperature, and η is the solvent viscosity. However, a problem arises; how does the size distribution of particles affect the determination of their diameter? This point will be discussed in this paper.

METHODS

As an introduction to our method, we first summarize our previous treatment for polydisperse suspensions of spherical shells (Fujime et al., 1988). Let $P(x)$ be the particle scattering function with $x = Kd/2$. The field correlation function of the scattered light averaged over a size distribution $N(z)$ with $z = d/d_n$ is given by

$$\langle g^1(\tau)\rangle = \frac{\int \exp[-D(d)K^2\tau]\ P(x)z^pN(z)\,dz}{\int P(x)z^pN(z)\,dz}, \quad (1)$$

where d_n is the number-average diameter, $D(d) = k_BT/(3\pi\eta d) = D(d_n)/z$, and $p = 4$ for shells with thin wall, and $p = 6$ for spheres. The time derivatives of Eq. 1 at $\tau = 0$ give

$$\langle D^1\rangle = \int D(d)^1z^pP(x)N(z)\,dz/\int P(x)z^pN(z)\,dz. \quad (2)$$

The average over $N(z)$ of the scattering function is given by

$$\langle P(x)\rangle = \int P(x)z^pN(z)\,dz/\int z^pN(z)\,dz. \quad (3)$$

To carry out integrations over z in Eqs. 2 and 3, the Schulz-Zimm distribution function without the normalization constant is assumed:

$$N(z) = z^m\exp[-(m+1)z]. \quad (4)$$

An integral formula valid for $(a, \alpha) > 0$ is useful in what follows;

$$\int_0^\infty \exp(-az)z^{\alpha-1}\cos(bz)\,dz = \frac{\Gamma(\alpha)}{(a^2+b^2)^{\alpha/2}}\cos[\alpha\tan^{-1}(b/a)]. \quad (5)$$

For spherical shells with wall thickness much smaller than the wavelength of the incident light, the particle scattering function is given by

$$P(x) = \sin^2(x)/x^2 \qquad \text{(valid for any size of the shell)} \quad (6)$$

We then have from Eqs. 2 (for $p = 4$), 4, and 6:

$$\frac{\langle D^i \rangle}{D(d_n)^i} = \frac{2(m+1)^i(m+2-i)!}{(m+4)!y^2\langle P(x)\rangle} \cdot [1 - \cos[(m+3-i)\tan^{-1}(y)]/(1+y^2)^{(m+3-i)/2}]; \quad (7)$$

$$(\mu_2/\Gamma^2) = \langle D^2\rangle/\langle D\rangle^2 - 1, \quad (8)$$

where $y = 2x_n/(m+1)$ with $x_n = Kd_n/2$, and μ_2 is the second cumulant in the cumulant expansion of $g^1(\tau)$. For $i = 0$, Eq. 7 gives $\langle P(x)\rangle$. Both $\langle D\rangle/D(d_n)$ and $(\mu_2/\bar{\Gamma}^2)$ show wiggling as functions of K^2 even for a highly monodisperse distribution, $m = 100$ (Fujime et al., 1988). This is graphically understood as follows: From Eqs. 2 (for $p = 4$) and 6, we have for $i = 1$

$$\langle D\rangle/D(d_n) = \int \sin^2(x_n z)zN(z)\,dz / \int \sin^2(x_n z)z^2N(z)\,dz. \quad (9)$$

For a unimodal $N(z)$, the integrands in Eq. 9 are unimodal or bimodal depending on x_n values as shown in Fig. 1. At $K^2 = 2 \cdot 10^{10}$ cm^{-2} (*left*), the heavy weight of $\sin^2(x_n z)$ for smaller particles results in a large D value. At $K^2 = 3 \cdot 10^{10}$ cm^{-2} (*right*), on the other hand, double peaks of the integrands result in a large $(\mu_2/\bar{\Gamma}^2)$ value. (For these, cf. Fig. 2 in Fujime et al., 1988.) The factor $x^2P(x)$ works as a notch filter to eliminate the contribution from particles with sizes around d which gives the minima of $x^2P(x) = \sin^2(x_n z)$. Since numerical results for spherical shells are detailed elsewhere (Fujime et al., 1988), we will not discuss

In what follows, we first extend the previous method to the case of polydisperse suspensions of spheres; we compare an approximate method in the Rayleigh-Debye regime with an exact one based on the Mie scattering theory. Then, characterization of isolated secretory granules is made by use of the present theoretical results.

RESULTS AND DISCUSSION

Theoretical Results for Spheres in the Rayleigh-Debye Regime

The particle scattering function for a sphere is given by

$$P(x) = [3\{\sin(x) - x\cos(x)\}/x^3]^2. \quad (10)$$

When "cos" on both sides of Eq. 5 is replaced with "sin," Eq. 5 holds as it is. From Eqs. 2 (for $p = 6$), 4, and 10, we easily obtain an analytic expression, Eq. 11, of $\langle D^i\rangle/D(d_n)^i$,

$$\frac{\langle D^i\rangle}{D(d_n)^i} = \frac{288(m-i)!(m+1)^i}{(m+6)!\,y^6\langle P(x)\rangle} \cdot [1 + (y/2)^2(m+2-i)(m+1-i) - \cos[(m+1-i)\tan^{-1}(y)]/(1+y^2)^{(m+1-i)/2} - y(m+1-i)\sin[(m+2-i) \cdot \tan^{-1}(y)]/(1+y^2)^{(m+2-i)/2} + (y/2)^2(m+2-i)(m+1-i)\cos[(m+3-i) \cdot \tan^{-1}(y)]/(1+y^2)^{(m+3-i)/2}] \quad (11)$$

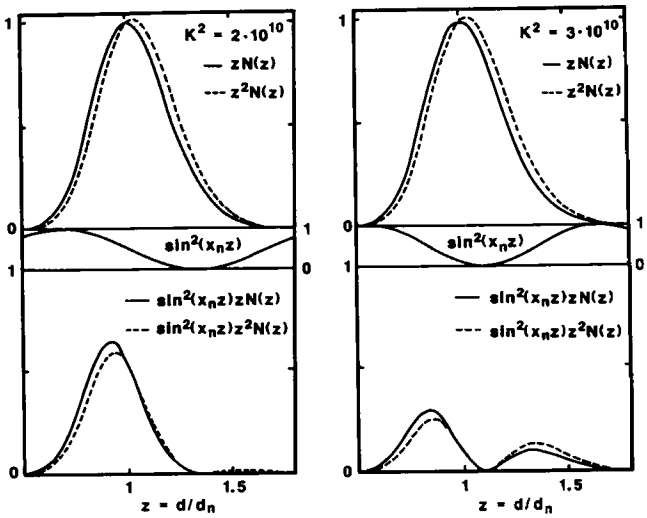

FIGURE 1. Illustration of the integrands in Eq. 9 for $d_n = 320$ nm and $m = 30$.

where $y = 2x_n/(m+1)$ as before. For $i = 0$, Eq. 11 gives $\langle P(x)\rangle$. Although lengthy, Eq. 11 is simple and its numerical computation can be performed by use of a programable calculator. Strictly speaking, however, it holds only for small particles, since $P(x)$ in Eq. 10 is derived in the Rayleigh-Debye regime. For large particles, the Mie scattering function $P_M(x)$ (see Appendix) has to be used instead of $P(x)$. "Large particles" here and hereafter mean the particles for which $2\pi|(n_1/n_2) - 1|(d/\lambda_0) \ll 1$ does not hold, where n_1 is the refractive index inside the particle. In our particular examples in this study, parameter values are $n_1/n_2 \sim 1.14$ and 300 nm $\leq d \leq$ 1,500 nm (or $0.7 \leq d/\lambda_0 \leq 3$). As shown in Fig. 2, the quasi-periodicity of $P(x)$ as a function of diameter is different from that of $P_M(x)$. If we put

$$d_{RD} = (1+\delta)d_M, \quad (12)$$

where the subscripts RD and M denote Rayleigh-Debye and Mie respectively, a value of $\delta = 0.07$ is found to be appropriate to adjust the positions of maxima and minima of both curves at $\theta = 60°$ (Fig. 2). At other angles, however, the peak positions gradually deviate from each other. In addition to this, the peak height of $P(x)$ with increase in diameter damps faster than that of $P_M(x)$. However, we first examine Eq. 11 for simulation of $\langle P(K)\rangle$ and $\langle D\rangle/D(d_n)$, because the most essential point in simulation is an oscillatory behavior of $P(x)$ against x as shown in Fig. 1. Computation by use of the Mie scattering function is given in the Appendix.

Comparison with Experimental Examples

The zymogen/chromaffin granule is one type of exocrine/endocrine granules, and is filled with amylase/catechol-

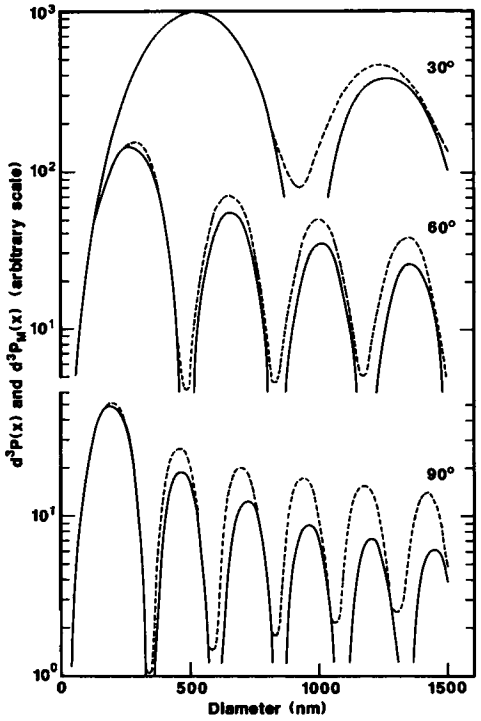

FIGURE 2. $d^3P(x)$ (*solid lines*) and $d^3P_M(x)$ (*dashed lines*) as a function of d for given values of θ (30, 60, and 90°), $\delta = 0.07$ (see Eq. 12), $n_1 = 1.51$, $n_2 = 1.33$, and $\lambda_0 = 488$ nm. See Appendix for the definition of the Mie scattering function $P_M(x)$. Both curves were normalized to 10^3 at the first peak at $\theta = 30°$. To avoid the cluttering, the ordinate for curves at $\theta = 90°$ is displaced from that for curves at $\theta = 30$ and 60°.

amine. These granules assume a sphere; the refractive indices inside and outside the granule are different from each other. Eq. 11 for $i = 0$ and 1 was numerically computed for zymogen ($d_n \sim 800$ nm) and chromaffin ($d_n \sim 400$ nm) granules. Fig. 3 shows the experimental and simulated results for zymogen granules. It should be noted that the experimental $K^2P(K)$ has a shoulder at $10^{-10}K^2 \sim 1.5$ cm^{-2}. This intensity profile can be simulated by Eq. 11 for $25 < m < 35$; Eq. 11 gives a prominent peak for $m \geq 40$, whereas it does not give even a shoulder for $m \leq 20$ (see the simulated lines in Fig. 3). We then have a rough estimate of $m \sim 30$. This value of m gives $\langle D \rangle / D(d_n)$ quite compatible with experimental results. The approximate form of $P(x)$ gives a good behavior of $\langle D \rangle / D(d_n)$ over the accessible range of K^2 because $P(x)$ appears in numerator and denominator of Eq. 2, whereas a poor behavior of $\langle P(x) \rangle$ at large K^2 (or large x) because the amplitude of oscillation in $P(x)$ damps faster than that in $P_M(x)$. Fig. 4 shows the experimental and simulated results for chromaffin granules. In this case, again, the fitting was good in $\langle D \rangle / D(d_n)$ but not in $K^2\langle P(K) \rangle$. The intensity profile for chromaffin granules did not give any definite range of m, as that for zymogen granules did. But, $\langle D \rangle / D(d_n)$ at $K^2 = 0$ strongly suggests that the m value is neither smaller than 15 nor larger than 40.

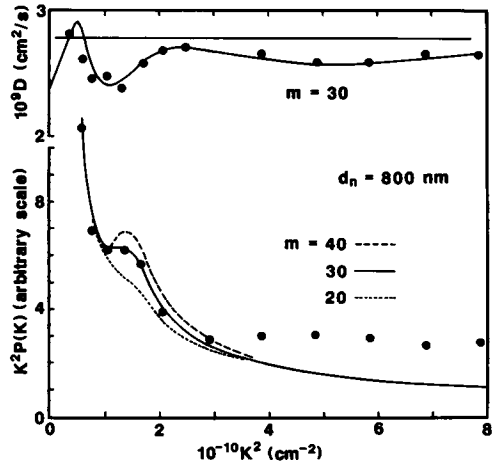

FIGURE 3. Experimental and simulated results for zymogen granules. The theoretical curves were based on Eq. 11 for $x_n = (1 + \delta)Kd_n/2$ with $\delta = 0.10$ (see Eq. 12). The horizontal line shows $\langle D \rangle / D(d_n) = 1.0$. Experimental data were obtained for a suspension of zymogen granules (~100 μg/ml protein) at 0.28 M sucrose, 5 mM 2-(*N*-morpholino) ethane sulfonic acid (pH 6.5), and 4 mM EGTA (Miyamoto and Fujime, manuscript in preparation).

Concluding Remarks

The weight, $z^pP(x)$, in the average of D is different from the weight, z^p, in the average of $P(x)$. Two parameters, m and d_n, of the size distribution, Eq. 4, can be determined rather rigorously, because a set of m and d_n should describe both $K^2P(K)$ vs. K^2 and D vs. K^2 relationships simultaneously.

The dispersion in the size distribution is given by $\sigma/d_n = [(\text{the mean of } d^2)/d_n^2 - 1]^{1/2} = (m + 1)^{-1/2}$, which is equal to 0.18 for $m = 30$. In both cases given above, the size

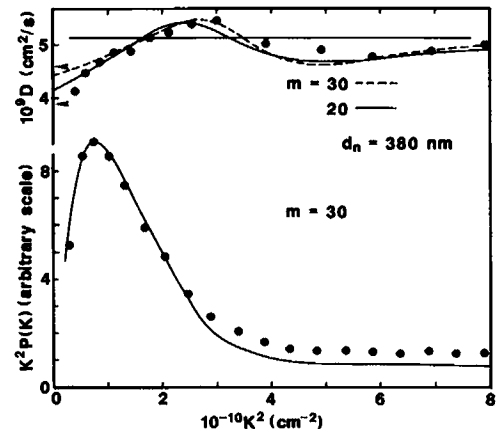

FIGURE 4. Experimental and simulated results for chromaffin granules. The theoretical curves were based on Eq. 11 for $\delta = 0.10$ (see legend to Fig. 3). The horizontal line shows $\langle D \rangle / D(d_n) = 1.0$. Arrows show $\langle D \rangle / D(d_n)$ at $K^2 = 0$ for $m = 40$ and 15. Experimental data were obtained for suspension of chromaffin granules (~100 μg/ml protein) at 0.30 M sucrose, 5 mM Hepes (pH 7.0), and 1 mM EGTA (Miyamoto and Fujime, 1988).

distribution of granules is concluded to be substantially monodisperse. Osmotic swelling studies of the zymogen and chromaffin granules will be given elsewhere (Miyamoto and Fujime, 1988, and manuscript in preparation).

As shown in the Appendix, when the Mie scattering function, $P_M(x)$, was used for $P(x)$ in Eq. 3, the behavior of $K^2\langle P(K)\rangle$ at large K^2 was substantially improved. However, no essential improvement was observed in the behavior of $\langle D\rangle/D(d_n)$ against K^2. If allowance is made for Eq. 12, our approximate method by use of Eq. 11 is then concluded to be very useful in simulation of characteristic behaviors of $K^2\langle P(k)\rangle$ and $\langle D\rangle/D(d_n)$ for large spheres, and in characterization of the scattering particles, as Eq. 7 does for spherical shells. Eq. 11 should first be examined, although machine computation of the Mie scattering function is now an easy task.

APPENDIX

Numerical Method for the Mie Scattering Function

When the electric field of the incident light is polarized normal to the scattering plane, the Mie scattering function for a sphere with diameter d is given as a function of θ (or K), d and $\mu = n_1/n_2$. The unnormalized scattering function $P_M(x)$, which corresponds to $P(x)$ in the Rayleigh-Debye regime, is given by

$$P_M(x) = |S_1(\theta, d, \mu)|^2/d^6, \quad (13)$$

where the scattering amplitude is given by (Kerker, 1969)

$$S_1(\theta, d, \mu) = -i\Sigma_\nu [A_\nu \sin(\nu\theta)/\sin(\theta) + \nu B_\nu \cos(\nu\theta)]. \quad (14)$$

In Eq. 13, a simplified notation $P_M(x)$ is used instead of $P_M(\theta, d, \mu)$, so that $P_M(x)$ should read "a function of d for given values of θ (or K), n_1, n_2, and λ_0" as in Fig. 2. A_ν and B_ν ($\nu = 1, 2, \ldots$) are given by $A_\nu = \Sigma_n Y^\nu_n a_n$ and $B_\nu = \Sigma_n Y^\nu_n b_n$, where $n = \nu, \nu + 2, \ldots$, and Y^ν_n is a simple function of integers n and ν. When the refractive index is real, the scattering coefficients are given by $a_n = \alpha_n/(\alpha_n - i)$ and $b_n = \beta_n/(\beta_n - i)$, where

$$\alpha_n = -[\psi'_n(\beta)\psi_n(\alpha) - \mu\psi_n(\beta)\psi'_n(\alpha)] / [\psi'_n(\beta)\chi_n(\alpha) - \mu\psi_n(\beta)\chi'_n(\alpha)] \quad (15a)$$

$$\beta_n = -[\mu\psi'_n(\beta)\psi_n(\alpha) - \psi_n(\beta)\psi'_n(\alpha)] / [\mu\psi'_n(\beta)\chi_n(\alpha) - \psi_n(\beta)\chi'_n(\alpha)] \quad (15b)$$

The size parameters are defined by $\alpha = (2\pi n_2/\lambda_0)d/2$ and $\beta = \mu\alpha$. Since $\psi_n(z) = zj_n(z)$, $\chi_n(z) = -(-1)^{n+1}zj_{-n-1}(z)$ and $j'_n(z) = dj_n(z)/dz = (n/z)j_n(z) - j_{n+1}(z)$, Eq. 15 can be written in terms of spherical Bessel functions $j_n(z)$ with various orders n. A previous algorithm (Fujime and Kubota, 1985; see also Abramowitz and Stegun, 1970) can easily compute $j_n(\alpha)$s for $n, n-1, \ldots$, and $-(n+1)$ simultaneously. Terms up to $\nu = 20$ were taken into account in Eq. 14.

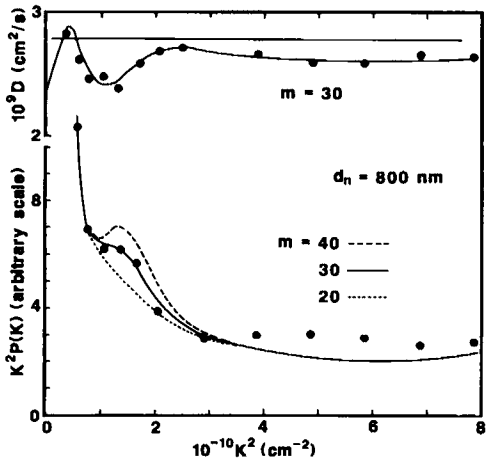

FIGURE 5. Experimental and simulated results for zymogen granules. The theoretical curves were based on the Mie scattering function. The horizontal line shows $\langle D\rangle/D(d_n) = 1.0$.

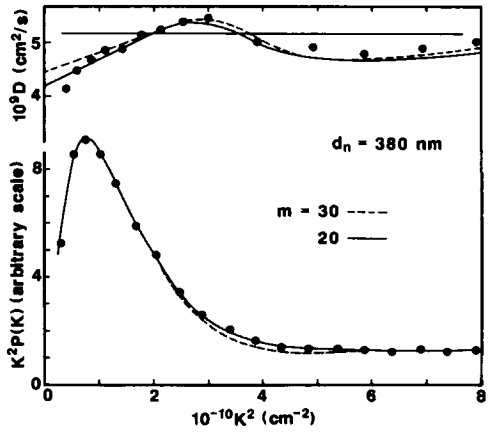

FIGURE 6. Experimental and simulated results for chromaffin granules. The theoretical curves were based on the Mie scattering function. The horizontal line shows $\langle D\rangle/D(d_n) = 1.0$.

Comparison with Experimental Examples

We do not know the size of n_1 inside the zymogen/chromaffin granule, and hence the size of μ. The refractive index of most proteins is 1.51, which gives $\mu = 1.13_5$ for $n_2 = 1.33$. This μ value will be its upper bound for zymogen granules in which protein (amylase) are densely packed. The dashed lines in Fig. 2 show the $d^3P_M(x)$ for $\mu = 1.13_5$. By use of Eqs. 2, 3, and 13, we simulated the results for zymogen (Fig. 5) and chromaffin granules (Fig. 6). In Fig. 5, the profile of $K^2\langle P(K)\rangle$ at large K^2 is improved as compared with that in Fig. 3. When a μ value larger than 1.14 was assumed, a more, but not an essential, improvement was observed. When $N(z)$ in Eq. 4 is assumed to be a mass distribution (and not the number distribution), p in Eqs. 1–3 should be 3. In this case, a substantial improvement was observed. This probably suggests that the skewness in the real distribution for zymogen granules is different from that of the assumed one. With increase in K^2, the quasiperiodicity of oscillation of both $P(x)$ and $P_M(x)$ becomes small (Fig. 2), so that the difference in skewness substantially affects the intensity profile at high K^2. In Fig. 6, on the other hand, the profile of $K^2\langle P(K)\rangle$ is almost completely improved. It should be noted that in both cases of zymogen and chromaffin granules, the behavior of $\langle D\rangle/D(d_n)$ against K^2 is almost the same as that of Eq. 11.

S. Miyamoto acknowledges the postdoctoral fellowship from Mitsubishi Kasei Institute of Life Sciences.

Received for publication 22 April 1988 and in final form 28 July 1988.

REFERENCES

Abramowitz, M., and I. A. Stegun. 1970. Handbook of Mathematical Functions with Formulas, Graphs and Mathematical Tables. 9th edition. Dover Publications Inc., New York. 1046 pp.

Berne, B., and R. Pecora. 1975. Dynamic Light Scattering. John Wiley & Sons, Inc., New York. 376 pp.

Chu, B. 1974. Laser Light Scattering. Academic Press, Inc., New York. 317 pp.

Fujime, S., and K. Kubota. 1985. Dynamic light scattering from dilute suspensions of thin discs and thin rods as limiting forms of cylinder, ellipsoid and ellipsoidal shell of revolution. *Biophys. Chem.* 23:1–13.

Fujime S., M. Takasaki-Ohsita, and S. Miyamoto. 1988. Dynamic light scattering from polydisperse suspensions of thin ellipsoidal shells of revolution with submicron diameters. *Biophys. J.* 53:497–503.

Kerker, M. 1969. The Scattering of Light and Other Electromagnetic Radiation. Academic Press, Inc., New York. 666 pp.

Li, W., T. S. Aurora, T. H. Haines, and H. Z. Cummins. 1986. Elasticity of synthetic phospholipid vesicles and submitochondrial particles during osmotic swelling. *Biochemistry.* 25:8220–8229.

Miyamoto, S., and S. Fujime. 1988. Regulation by Ca^{2+} of membrane elasticity of bovine chromaffin granules. *FEBS (Fed. Eur. Biochem. Soc.) Lett.* In press.

Miyamoto, S., T. Maeda, and S. Fujime. 1988. Change in membrane elastic modulus on activation of glucose transport system of brush border membrane vesicles studied by osmotic swelling and dynamic light scattering. *Biophys. J.* 53:505–512.